Plasmonics in argentene

Ravishankar Sundararaman,[1,*] Thomas Christensen,[2] Yuan Ping,[3] Nicholas Rivera,[2,4] John D. Joannopoulos,[2] Marin Soljačić,[2] and Prineha Narang[4,†]

[1]*Department of Materials Science and Engineering, Rensselaer Polytechnic Institute, Troy, New York 12180, USA*
[2]*Department of Physics, Massachusetts Institute of Technology, Cambridge, Massachusetts 02139, USA*
[3]*Department of Chemistry, University of California, Santa Cruz, California 95064, USA*
[4]*John A. Paulson School of Engineering and Applied Sciences, Harvard University, Cambridge, Massachusetts 02138, USA*

(Received 14 November 2018; accepted 29 April 2020; published 24 July 2020)

Merging concepts from the fields of *ab initio* materials science and nanophotonics, there is now an opportunity to engineer new photonic materials whose optical, transport, and scattering properties are tailored to attain thermodynamic and quantum limits. Here we present first-principles calculations predicting that *Argentene*, a single-crystalline hexagonal close-packed monolayer of Ag, can dramatically surpass the optical properties and electrical conductivity of conventional plasmonic materials. In the low-frequency limit, we show that the scattering rate and resistivity reduce by a factor of 3 compared to the bulk three-dimensional metal. Most importantly, the low scattering rate extends to optical frequencies in sharp contrast to, e.g., graphene, whose scattering rate increase drastically in the near-infrared range due to optical-phonon scattering. Combined with an intrinsically high carrier density, this facilitates highly confined surface plasmons extending to visible frequencies. We evaluate Argentene across three distinct figures of merit, in each outperforming the state-of-the-art, making it a valuable addition to the two-dimensional heterostructure toolkit for quantum optoelectronics.

DOI: 10.1103/PhysRevMaterials.4.074011

Frontiers in the science of quantum materials increasingly focus on novel phenomena and properties that emerge in the limit of extreme quantum confinement and low dimensionality [1–16]. The surface plasmon resonance of two-dimensioanl (2D) and ultrathin conductors exhibits a drastically different dispersion relation from bulk three-dimensional (3D) conductors, with an order of magnitude higher-mode confinement [17]. Consequently, 2D materials are expected to introduce a paradigm shift by condensing optical phenomena to the atomic-scale, enabling strong interaction between quantum emitters and plasmons [18,19]. However, the low intrinsic carrier densities and strong optical-phonon scattering in known 2D conductors so far limit the regime of low-loss 2D plasmonics to midinfrared frequencies [20].

Delivering the promise of 2D nanophotonics [21,22] to the visible region while retaining low loss and long propagation lengths, requires true 2D metals with carrier densities two orders of magnitude higher than present-day 2D conductors (which are doped semi-metals) and semiconductors, and without optical-phonon losses. Model calculations of single-layer Ag and Au treat the hypothetical 2D metal as a 2D electron gas at the jellium level [23], or as a conductive sheet with properties extrapolated from the bulk dielectric function [6,24,25]. However, there are two fundamental limitations with previous model calculations. First, the all-important scattering time that determines loss in the material is unknown and treated as an empirical parameter, at best extrapolated from its the bulk value, while scattering times in deposited thin films of metals decrease with film thickness [26–28]. Second, and more importantly, it is unclear from previous model calculations if the material would remain stable in its monolayer form.

Our work overcomes these fundamental limitations in the literature to calculate a new class of monolayer plasmonic metals. Here, we use *ab initio* calculations to show that a monolayer of Ag atoms can form a stable 2D hexagonal close-packed lattice, which we henceforth refer to as Argentene. Furthermore, from first-principles electron-phonon scattering calculations, we predict that the momentum relaxation time in single-crystalline Argentene not only matches the value of perfect bulk Ag, but that it, in fact, exceeds it by a factor of 3. Correspondingly, the conductivity of Argentene is three times larger than bulk Ag and is comparable to the best-case optimally doped values for graphene. Finally, we show that Argentene particularly shines in its optical response because the absence of optical-phonon scattering allows the high relaxation time to persist to high frequencies, unlike in graphene where it sharply drops off past 0.2–0.5 eV photon energies.

Argentene, a single close-packed atomic layer of Ag atoms, exhibits the band structure of a nearly perfect 2D electron gas for electrons near the Fermi level, as shown in our density functional theory (DFT) calculations [29] in Fig. 1(a). The quadratic dispersion relation is disrupted by d-bands that start 3.5 eV below the Fermi level, remarkably similar to 3D bulk Ag. Charge transport in Argentene is, however, markedly different from bulk Ag. The electron-phonon scattering time, which critically determines electrical conductivity and plasmonic quality factors, to be a factor of 3 larger in Argentene as shown in Fig. 1(b). Electron-electron scattering contributes

*sundar@rpi.edu
†prineha@seas.harvard.edu

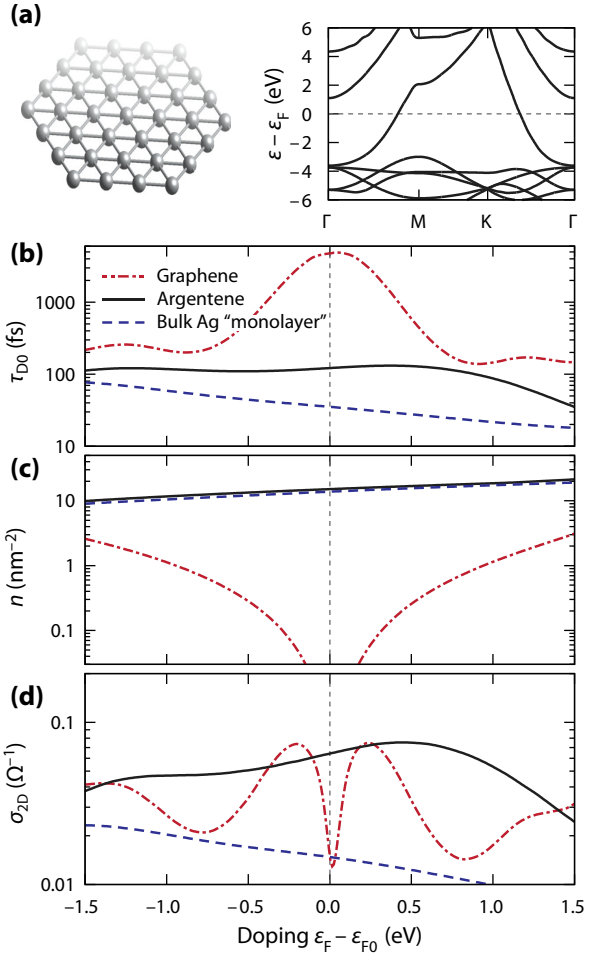

FIG. 1. Structure and DC carrier transport in Argentene: (a) Argentene is a single hexagonal-close packed atomic layer of Ag with a 2D electron-gas-like band structure extending till the *d*-bands 3.5 eV below the Fermi level. (b) Electron-phonon momentum relaxation time for DC transport, τ_{D0} in Argentene is three times larger than bulk Ag, and nominally independent of the Fermi level position, and is comparable to that of heavy ideally doped graphene (no dopant scattering). (c) Argentene's carrier density is an order of magnitude greater than graphene at practical doping levels, resulting in (d), a larger 2D conductivity through most of the relevant range. [For comparison, results for the bulk Ag "monolayer" in (c) and (d) are normalized to a thickness equal to its (111)-layer separation $t_{2D} \approx 2.36$ Å.]

negligibly to momentum relaxation at the Fermi surface with $\tau_{ee} \approx 1400\,\text{fs} \gg \tau_{D0}$ at 300 K [30,31], and therefore does not affect the conductivity or plasmonic properties. Note that conventional expectations from charge transport in thin *imperfect* films of noble metals that scattering time decreases with film thickness is due to surface and grain boundary scattering [26–28]. Here we focus on the potential of the ideal material and consistently compare results for perfect single crystals in both the 2D and 3D cases. Similarly, we do not consider substrate screening or loss, focusing instead on the intrinsic plasmonic properties of the free-standing monolayers. Throughout this paper we compare Argentene and graphene for concreteness, motivated by graphene's prominent position in 2D plasmonics.

Perfect undoped graphene exhibits scattering time exceeding picoseconds [Fig. 1(b)], but a low carrier density [Fig. 1(c)] and hence only a modest 2D conductivity [Fig. 1(d)]. Making graphene into a useful conductor or plasmonic material requires doping to increase the carrier density, but this also increases the density of states at the Fermi level ε_F and the phase-space for electron-phonon scattering, resulting in a reduction in scattering time with increasing carrier concentration. This results in a peak 2D conductivity of 0.06 Ω^{-1} at an optimal doping level that corresponds to a Fermi level 0.3 eV away from the Dirac point and a carrier density $n \sim 0.1\,\text{nm}^{-2} = 10^{13}\,\text{cm}^{-2}$. For a fair comparison with single-crystal Argentene, we consider ideal doping in graphene, i.e., neglect any impact of dopant scattering to provide a best-case scenario for graphene. Argentene matches this best-case 2D conductivity of 0.06 Ω^{-1} without need for doping.

For comparison, we also show predictions for Argentene with Fermi levels tuned away from neutrality ε_{F0} (e.g., by doping) and find that its properties are virtually unchanged. We additionally include calculations for a *bulk* Ag "monolayer," corresponding to a slab with bulk Ag's material properties and a thickness equal to its (111)-layer separation $t_{2D} \approx 2.36$ Å; this is effectively a classical down-extrapolation of bulk properties to the monolayer domain. The scattering time is nearly constant with the change of Fermi level, consistent with the flat density of states, and hence phase space for electron phonon scattering, of a 2D free-electron system. [The reduction near $\varepsilon_F - \varepsilon_{F0} \sim 1$ eV is due to an unoccupied band about 1-eV above the Fermi level, as shown in Fig. 1(a)]. The scattering time decreases with increasing Fermi level in bulk Ag due to $g(\varepsilon) \propto \sqrt{\varepsilon}$ for a 3D free-electron system, while in graphene, it decreases as the Fermi level moves away from the Dirac point (at energy ε_0) due to the increase in the density of states as $g(\varepsilon) \propto |\varepsilon - \varepsilon_0|$. We reiterate that Argentene does not require doping since it is a true 2D metal, whereas graphene is a semi-metal (conversely, Argentene's optical properties are less tunable by doping than graphene's), and all subsequent results focus on undoped Argentene. Similarly, for comparison, we focus on undoped bulk Ag and graphene at its best-case ideal doping of 0.3–0.5 eV.

Next, *ab initio* DFT calculations show that Argentene is mechanically stable as a free-standing 2D material, indicated by the absence of any imaginary frequencies in the phonon band structure in Fig. 2(a). Figure 2(b) reinforces this by showing the barrier for an atom in the plane of Argentene to hop onto the next layer [Fig. 2(c)], representative of the process by which a single monolayer could fragment into clusters or multilayers. We find a kinetic barrier of 0.16 eV ($\approx 6k_BT$ at room temperature) for free-standing Argentene; this can be doubled when bound to a van der Waals substrate (e.g., hexagonal boron nitride) with a modest binding energy per atom ~ 0.2 eV. While these calculations support that Argentene can be thermodynamically stable as large-scale crystals, they do not unambiguously establish it. However, recent experimental findings [32,33] already demonstrated the feasibility of isolating single- or few-layer silver crystals.

Transitioning from DC and low-frequency transport properties to the optical and plasmonic response of metals, the relevant material response function is the frequency-dependent

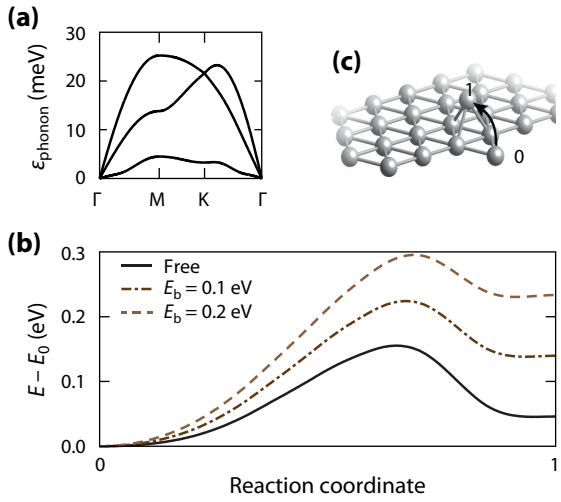

FIG. 2. Stability of Argentene from first-principles. (a) Phonon bandstructure without imaginary frequencies indicate a mechanically stable 2D layer. (b) Kinetic stability towards island formation, evaluated using the barrier for an in-plane atom to jump on top of the 2D layer; path is sketched in (c). The 0.16-eV barrier for free-standing Argentene increases as the binding energy per atom E_b to a hypothetical van der Waals substrate increases, allowing the single atomic layer to be further stabilized on an appropriately chosen substrate.

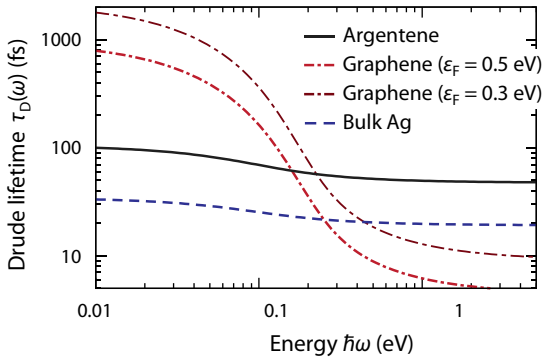

FIG. 3. Frequency-dependence of momentum-relaxation time. The electron-phonon momentum (Drude) relaxation time $\tau_D(\omega)$ of graphene (Fermi levels $\varepsilon_F = 0.3$ and 0.5 eV) is initially substantially higher than Ag and Argentene in the low-frequency limit, but drops dramatically at frequencies above 0.2 eV, falling below that of Argentene and Ag due to strong optical-phonon scattering in graphene. Argentene's relaxation time is consistently three times larger than bulk Ag; both exhibit only minor reduction with increasing frequency due to the absence of an analogous optical-phonon scattering mechanism in these materials.

complex conductivity (closely related to the dielectric function via $\sigma(\omega) = -i\omega[\epsilon(\omega) - \epsilon_0]$), which can be written as [34]

$$\sigma(\omega) = \frac{\sigma_0 \tau_{D0}^{-1}}{\tau_D^{-1}(\omega) - i\omega} + \sigma_d(\omega), \tag{1}$$

where σ_0 and τ_{D0} are the DC conductivity and Drude momentum-relaxation time, $\tau_D(\omega)$ is the frequency-dependent momentum relaxation time that encapsulates intraband phonon-assisted contributions to the optical response, and $\sigma_d(\omega)$ is the contribution due to direct optical transitions. We emphasize all of these quantities are calculated from a fully first-principles treatment of electrons and phonons, explicitly including all bands, modes, and coupling matrix elements, as discussed in Supplemental Material Ref. [22]. For 2D materials, we consider the corresponding 2D conductivities (σ_{2D}) rather than the bulk conductivities (σ).

The frequency-dependent relaxation time $\tau_D(\omega)$ directly determines the intraband loss, which along with interband losses in $\sigma_d(\omega)$, limit the plasmonic performance. Figure 3 shows that graphene's DC relaxation time drops by two orders of magnitude in the 0.2–0.5 eV frequency window due to scattering with optical phonons with a maximum energy ~ 0.2 eV. In contrast, both bulk Ag and Argentene do not have optical phonons and show a much more modest reduction in their relaxation times, around a factor of 2, from DC to optical frequencies. This leads to a cross-over at ~ 0.2 V, where Argentene takes over as the lower-loss material. This low-loss regime persists well into the visible region up to the interband threshold ~ 3.5 eV in both Argentene and Ag, beyond which direct transitions generate high losses.

The plasmon dispersion of a given 2D layer is directly related to the frequency-dependent 2D conductivity $\sigma_{2D}(\omega)$. Specifically, the in-plane plasmon wave vector q disperses with frequency as $q = [(2i\varepsilon_0\omega/\sigma_{2D})^2 + k_0^2]^{1/2}$ (free-space wave vector, $k_0 \equiv \omega/c$), reducing to $q \simeq 2i\varepsilon_0\omega/\sigma_{2D}$ in the quasistatic limit [7,35,36]. Figure 4 depicts the plasmon dispersion of of Argentene, doped graphene, and nanometric slabs of bulk Ag of thickness t [spanning integer-multiples of Ag's (111)-layer separation $t_{2D} \approx 2.36$ Å]. The plasmon's dispersion coincides with the peaks of the imaginary part of the transverse-magnetic (TM) reflection coefficient [Fig. 4(a)]; the associated peak width relates directly with the plasmon lifetime and propagation length.

At small excitation energies, the 2D layers exhibit the well-known $\omega \underset{\sim}{\propto} q^{1/2}$ dispersion. This furnishes them with substantially larger wave vectors (at fixed frequency)—and hence stronger confinement—than their finite-thickness slab counterparts [Fig. 4(b)]. Given the manifold opportunities facilitated by high confinement, the attraction of the monolayer limit is manifest: confinement is more than an order of magnitude larger in Argentene than the 16-layer Ag slab. The enhancement is immediately appreciable from a small-thickness analysis of the slab's dispersion equation [37], which demonstrates that, classically, $q(\omega) \underset{\sim}{\propto} 1/t$ for $t \ll k_0 \ll |q|$. Coincidentally, the dispersion $\mathrm{Re}\, q(\omega)$ of the Ag slab of thickness $t = t_{2D}$, i.e., the "monolayer" bulk Ag slab (ML-Ag), exhibits a counterintuitively good agreement with Argentene. This, however, is expected: for a 2D carrier density n, the plasmon dispersion is $\mathrm{Re}\, q \underset{\sim}{\propto} \omega^2/n^s$ in the Drude regime (with $s = 1$ in metals and $s = 1/2$ in graphene, cf. its Dirac dispersion) [36]. Accordingly, the observed agreement merely reflects the approximate equality of n in Argentene and $n_{3D}t_{2D}$ in ML-Ag. Argentene distinguishes itself from graphene in two ways. (1) Plasmon frequencies exceed graphene's significantly, extending into the NIR and above, and

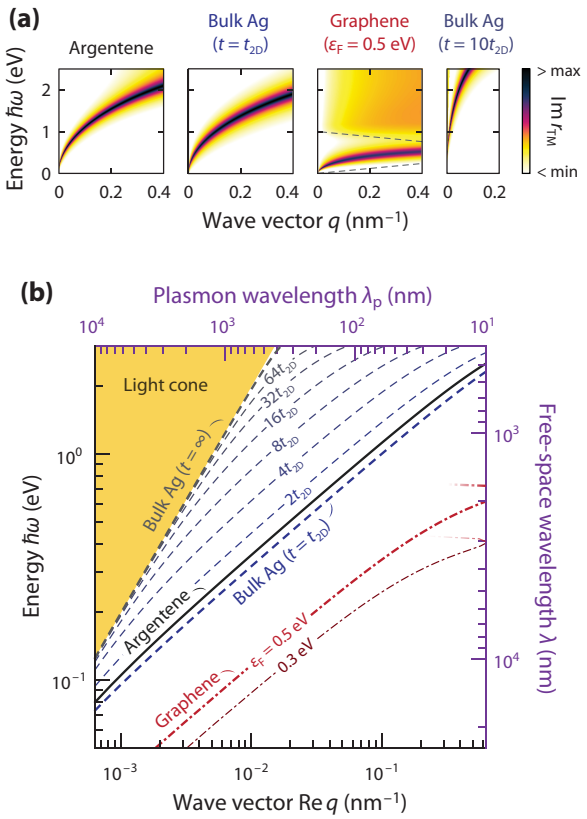

FIG. 4. Plasmon dispersion of Argentene, doped graphene ($\varepsilon_F = 0.3$ and 0.5 eV), and thin slabs of bulk Ag. (a) Imaginary part of the TM reflectivity Im r_{TM} (logarithmic, clamped colorscale) whose peaks reflect the existence of plasmon modes. (b) Corresponding plasmon dispersion (solved for complex q and real ω) for Argentene, graphene, and bulk Ag slabs (thicknesses range over $t = 2^n t_{2D}$ for $n = 0, 1, \ldots, 6$, and ∞). The confinement of Argentene plasmons agree well with that predicted from down-extrapolation of bulk Ag's properties to a monolayer's thickness.

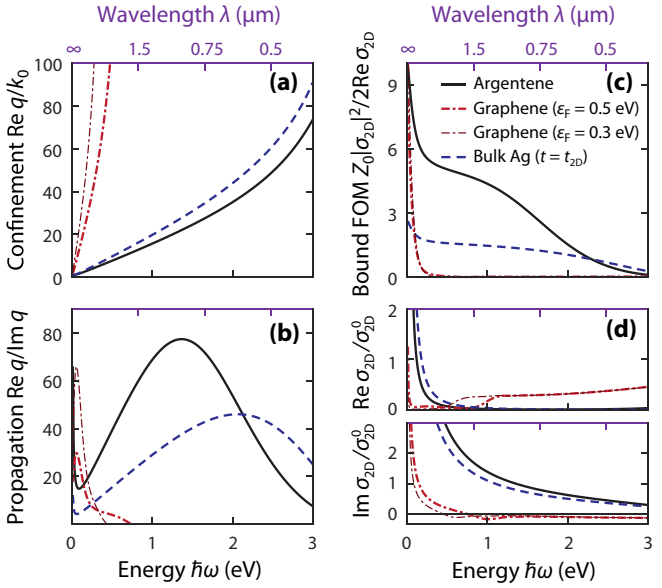

FIG. 5. Plasmonic figures of merit in Argentene, doped graphene ($\varepsilon_F = 0.3$ and 0.5 eV), and "monolayer" bulk Ag. (a) Confinement ratio Re q/k_0. (b) Effective propagation length Re q/Im q. (c) Bound-related FOM $\Omega \equiv Z_0|\sigma_{2D}|^2/2\,\mathrm{Re}\,\sigma_{2D}$. (d) Real and imaginary parts of the 2D conductivity σ_{2D} (in units of $\sigma^0_{2D} \equiv e^2/\hbar$). Argentene offers roughly an order of magnitude increase in maximal effective propagation length over graphene—whose response above 0.2 eV (below 6 μm) is dominated by electron-phonon interaction with its optical phonon branch—similar confinement ratios, and superior bound-FOM. Argentene's plasmonic properties are optimal near the 1.55-μm telecommunication band. Relative to bulk-extrapolated monolayer properties, i.e., to bulk Ag slabs of thickness $t = t_{2D}$, Argentene exhibits anomalously improved plasmonic attributes.

(2) confinement is smaller at equal frequencies. Since $\mathrm{Re}\,q \propto 1/n^s$, both differences are consequences of Argentene's higher carrier density n. The cost of larger n, however, is a reduced tunability of n—and hence of plasmon frequencies—e.g., by external gating, cf. Fig. 1(c) (unlike graphene, which is highly tunable).

In Figs. 5(a) to 5(c), we consider three distinct figures of merit (FOMs), spanning the gamut of typical plasmonic applications: confinement ratio Re q/k_0, effective propagation length Re q/Im q, and a bound-related FOM $\Omega \equiv Z_0|\sigma_{2D}|^2/2\,\mathrm{Re}\,\sigma_{2D}$ (Z_0, impedance of free space) [25]. The later FOM warrants further explication than the previous two, which are well-established plasmonic FOMs: Ω bounds the optical response of arbitrarily shaped 2D resonators—e.g., the extinction efficiency is $\leqslant 2\Omega$, the Purcell factor is $\leqslant \frac{3}{4}(k_0 d)^{-4}\Omega$, and the radiative heat flux (between identical bodies) relative to the black-body limit is $\leqslant 6(k_0 d)^{-4}\Omega^2$, for emitter–body and body–body separations d. In the quasistatic limit, the bound-related FOM is $\Omega \simeq k_0/\mathrm{Im}\,q$, i.e., a complementary effective propagation length, taken relative to its free-space wavelength. Interestingly, the two conventional FOMs, confinement ratio and effective propagation length, are also simply related to the conductivity in the quasistatic limit: $\mathrm{Re}\,q/\mathrm{Im}\,q \simeq \mathrm{Im}\,\sigma_{2D}/\mathrm{Re}\,\sigma_{2D}$ and $\mathrm{Re}\,q/k_0 \simeq 2\,\mathrm{Im}\,\sigma_{2D}/Z_0|\sigma_{2D}|^2$. Thus, each FOM convey, approximately, distinct ratios of the complex components of the conductivity [Fig. 5(d)].

Despite these commonalities, the three FOMs individually present contrasts. In terms of confinement [Fig. 5(a)] doped graphene surpasses Argentene, while Argentene and ML-Ag agree well. Conversely, graphene's propagation ratios [Fig. 5(b)] fall short of Argentene's, except in the low-frequency region ($\lesssim 0.2$ eV). Similarly, the propagation ratios of Argentene and ML-Ag exhibit significant discrepancies. Analogous observations are evident for the bound-related FOM [Fig. 5(c)]. This FOM-dependent contrast between Argentene and ML-Ag conclusions reflects a fundamental difference in the essential dependence of each FOM: confinement, on one hand, is a comparatively simple theoretical construct, depending mainly on macroscopic properties, specifically the carrier density n, as discussed previously. On the other hand, propagation ratios (and the bound-related FOM) sensitively depend on relaxation mechanisms, which are intrinsically microscopic. Specifically, relaxation can occur either through direct transitions [38] or through electron-phonon interactions. These interactions are incorporated here via a frequency-dependent relaxation time $\tau(\omega)$, computed

from the Eliashberg spectral function. The discrepancy between ML-Ag and Argentene underscores the need for full, microscopic accounts of the electron-phonon interaction in the quantitative assessment of novel 2D plasmonic materials.

The preceding discussion also explains the differences noted between graphene and Argentene: graphene's confinement exceeds Argentene's due to its lower carrier density, at the cost of lower operation frequencies. In contrast, the operation range of graphene's plasmons is further restricted in practice due to the onset of strong electron-phonon interaction with graphene's optical phonon branch at 0.2 eV [6,39]. At room temperature, this interaction significantly broadens graphene's plasmons, near and above the threshold (at cryogenic temperatures, strong relaxation is thresholded to energies $\gtrsim 0.2$ eV, with $\mathrm{Im}\, q$ decreased markedly below). Argentene, a single-atom Bravais lattice, does not support optical phonons and consequently is not similarly impacted. Jointly, the three FOMs of Figs. 5(a) to 5(c) underscore the appeal of Argentene for plasmonics, and the importance of microscopic accounts in theoretical assessments of novel plasmonic materials.

In summary, our first-principles calculations reveal that Argentene, a single hexagonal close-packed atomic-layer of Ag, is mechanically stable in free-standing form and exhibits three-times the momentum relaxation time and conductivity as bulk Ag, comparable to the best-case scenario for ideally doped graphene. While graphene's long scattering time and low-loss regime are limited to frequencies $\hbar\omega \lesssim 0.2\,\mathrm{eV}$ due to optical-phonon scattering, Argentene's low-loss regime extends well into the visible spectrum, up to an interband threshold $\sim 3.5\,\mathrm{eV}$. Consequently, Argentene exhibits highly confined plasmons with long propagation lengths at much higher frequencies. Looking forward, realizing the promise of ultra-confined, long-lived, visible-spectrum 2D plasmonics with Argentene requires the identification of suitable substrates and techniques to reliably grow single-crystal noble-metal monolayers [40–45] that simultaneously retain the electron-phonon scattering properties.

The authors thank Prof. Efthimios Kaxiras (Harvard University), Prof. John Pendry (Imperial College, London), Prof. Ling Lu (Chinese Academy of Science), Prof. Toh-Ming Liu (RPI), and Prof. Daniel Gall (RPI) for fruitful discussions on 2D plasmonic materials, potential monolayer growth techniques, and carrier scattering properties. R.S. acknowledges start-up funding from the Department of Materials Science and Engineering at Rensselaer Polytechnic Institute. T.C. acknowledges support from the Danish Council for Independent Research (Grant No. DFF–6108-00667). N.R. was supported by Department of Energy Fellowship DE-FG02-97ER2530 (DOE CSGF). The research of J.D.J. and M.S. was supported as part of the Army Research Office through the Institute for Soldier Nanotechnologies under Contract No. W911NF-18-2-0048 (photon management for developing nuclear-TPV and fuel-TPV mm-scale-systems), and also supported as part of the S3TEC, an Energy Frontier Research Center funded by the US Department of Energy under Grant No. DE-SC0001299 (for fundamental photon transport related to solar TPVs and solar-TEs). P.N. acknowledges start-up funding from the Harvard John A. Paulson School of Engineering and Applied Sciences. This research used resources of the National Energy Research Scientific Computing Center, a DOE Office of Science User Facility supported by the Office of Science of the US Department of Energy under Contract No. DE-AC02-05CH11231, the Research Computing Group at Harvard University as well as resources at the Center for Computing Innovations (CCI) at Rensselaer Polytechnic Institute.

[1] K. S. Novoselov, D. Jiang, F. Schedin, T. J. Booth, V. V. Khotkevich, S. V. Morozov, and A. K. Geim, Proc. Natl. Acad. Sci. USA **102**, 10451 (2005).
[2] Y. Cao, V. Fatemi, S. Fang, K. Watanabe, T. Taniguchi, E. Kaxiras, R. C. Ashoori, and P. Jarillo-Herrero, Nature **556**, 43 (2018).
[3] Y. Cao, V. Fatemi, A. Demir, S. L. Fang, S. Tomarken, J. Y. Luo, J. D. Sanchez-Yamagishi, K. Watanabe, T. Taniguchi, E. Kaxiras, R. C. Ashoori, and P. Jarillo-Herrero, Nature **556**, 80 (2018).
[4] M. N. Gjerding, P. Mohnish, and K. S. Thygesen, Nat. Commun. **8**, 15133 (2016).
[5] K. Andersen, S. Latini, and K. S. Thygesen, Nano Lett. **15**, 4616 (2015).
[6] M. Jablan, M. Soljačić, and H. Buljan, Proc. IEEE **101**, 1689 (2013).
[7] Y. V. Bludov, A. Ferreira, N. M. R. Peres, and M. I. Vasilevskiy, Int. J. Mod. Phys. B **27**, 1341001 (2013).
[8] F. J. García de Abajo, ACS Photonics **1**, 135 (2014).
[9] T. Stauber, J. Phys.: Condens. Matter **26**, 123201 (2014).
[10] T. Low and P. Avouris, ACS Nano **8**, 1086 (2014).
[11] T. Low, J. D. Chaves, A. Caldwell, A. Kumar, N. X. Fang, P. Avouris, T. F. Heinz, F. Guinea, L. Martin-Moreno, and F. Koppens, Nat. Mater. **16**, 182 (2017).
[12] D. N. Basov, M. M. Fogler, and F. J. García de Abajo, Science **354**, aag1992 (2016).
[13] P. Narang, L. Zhao, S. Claybrook, and R. Sundararaman, Adv. Opt. Mater. **5**, 1600914 (2017).
[14] G. T. Papadakis, P. Narang, R. Sundararaman, N. Rivera, H. Buljan, N. Engheta, and M. Soljačić, ACS Photonics **5**, 384 (2018).
[15] K. Sadhukhan and A. Agarwal, Phys. Rev. B **96**, 035410 (2017).
[16] Y. Huang, S. N. Shirodkar, and B. I. Yakobson, J. Am. Chem. Soc. **139**, 17181 (2017).
[17] S. N. Shirodkar, M. Mattheakis, P. Cazeaux, P. Narang, M. Soljačić, and E. Kaxiras, Phys. Rev. B **97**, 195435 (2018).
[18] D. Alcaraz Iranzo, S. Nanot, E. J. C. Dias, I. Epstein, C. Peng, D. K. Efetov, M. B. Lundeberg, R. Parret, J. Osmond, J.-Y.. Hong, J. Kong, D. R. Englund, N. M. R. Peres, and F. H. L. Koppens, Science **360**, 291 (2018).
[19] J. Mertens, M.-E. Kleemann, R. Chikkaraddy, P. Narang, and J. J. Baumberg, Nano Letters, Nano Lett. **17**, 2568 (2017).

[20] G. X. Ni, A. S. McLeod, Z. Sun, L. Wang, L. Xiong, K. W. Post, S. S. Sunku, B.-Y.. Jiang, J. Hone, C. R. Dean, M. M. Fogler, and D. N. Basov, Nature **557**, 530 (2018).
[21] J. Pendry, Science **285**, 1687 (1999).
[22] J. B. Khurgin, Faraday Discuss. **178**, 109 (2015).
[23] A. Manjavacas and F. J. García de Abajo, Nat. Commun. **5**, 3548 (2014).
[24] F. J. García de Abajo and A. Manjavacas, Faraday Discuss. **178**, 87 (2015).
[25] O. D. Miller, O. Ilic, T. Christensen, M. T. H. Reid, H. A. Atwater, J. D. Joannopoulos, M. Soljačić, and S. G. Johnson, Nano Lett. **17**, 5408 (2017).
[26] K. Fuchs, Math. Proc. Cambridge Phil. Soc. **34**, 100 (1938).
[27] E. H. Sondheimer, Adv. Phys. **1**, 1 (1952).
[28] T. Zhou, P. Zheng, S. C. Pandey, R. Sundararaman, and D. Gall, J. Appl. Phys. **123**, 155107 (2018).
[29] See Supplemental Material at http://link.aps.org/supplemental/10.1103/PhysRevMaterials.4.074011 for (i) *ab initio* computational details, (ii) theoretical frameworks for calculation of low- and finite-frequency conductivities and relaxation rates, and (iii) plasmon dispersion equations (includes Refs. [7,30,35–37,46–56]).
[30] A. M. Brown, R. Sundararaman, P. Narang, W. A. Goddard, III, and H. A. Atwater, ACS Nano **10**, 957 (2016).
[31] A. M. Brown, R. Sundararaman, P. Narang, A. M. Schwartzberg, W. A. Goddard, III, and H. A. Atwater, Phys. Rev. Lett. **118**, 087401 (2017).
[32] D. Kong and J. Druckner, J. Appl. Phys. **114**, 144310 (2013).
[33] Z. M. Abd El-Fattah, V. Mkhitaryan, J. Brede, L. Fernandez, C. Li, Q. Guo, A. Ghosh, A. Rodriguez Echarri, D. Naveh, F. Xia, J. Enrique Ortega, and F. Javier García de Abajo, ACS Nano **13**, 7771 (2019).
[34] The conductivity of Argentene is isotropic within the local-response limit due to its triangular symmetry.
[35] F. H. L. Koppens, D. E. Chang, and F. J. García de Abajo, Nano Lett. **11**, 3370 (2011).
[36] T. Christensen, *From Classical to Quantum Plasmonics in Three and Two Dimensions* (Springer, New York, 2017).
[37] E. N. Economou, Phys. Rev. **182**, 539 (1969).
[38] Our calculations neglect beyond-local response mechanisms, such as intraband Landau damping. Their impact on the charge-symmetric mode is negligible [57], except at higher wave vectors beyond those considered here.
[39] M. Jablan, H. Buljan, and M. Soljačić, Phys. Rev. B **80**, 245435 (2009).
[40] M.-H. Schaffner, F. Patthey, and W.-D. Schneider, Surf. Sci. **417**, 159 (1998).
[41] Q. Ma and D. R. Clarke, J. Mater. Res. **10**, 853 (1995).
[42] W. Chen, M. D. Thoreson, S. Ishii, A. V. Kildishev, and V. M. Shalaev, Opt. Express **18**, 5124 (2010).
[43] X. Huang, Z. Zeng, S. Bao, M. Wang, X. Qi, Z. Fan, and H. Zhang, Nat. Commun. **4**, 1444 (2013).
[44] K. M. McPeak, S. V. Jayanti, S. J. P. Kress, S. Meyer, S. Iotti, A. Rossinelli, and D. J. Norris, ACS Photonics **2**, 326 (2015).
[45] P. Nagpal, N. C. Lindquist, S.-H. Oh, and D. J. Norris, Science **325**, 594 (2009).
[46] R. Sundararaman, K. Letchworth-Weaver, K. A. Schwarz, D. Gunceler, Y. Ozhabes, and T. A. Arias, SoftwareX **6**, 278 (2017).
[47] M. Schlipf and F. Gygi, Comput. Phys. Commun. **196**, 36 (2015).
[48] J. P. Perdew, K. Burke, and M. Ernzerhof, Phys. Rev. Lett. **77**, 3865 (1996).
[49] R. Sundararaman and T. A. Arias, Phys. Rev. B **87**, 165122 (2013).
[50] S. L. Dudarev, G. A. Botton, S. Y. Savrasov, C. J. Humphreys, and A. P. Sutton, Phys. Rev. B **57**, 1505 (1998).
[51] R. Sundararaman, P. Narang, A. S. Jermyn, W. A. Goddard, III, and H. A. Atwater, Nat. Commun. **5**, 5788 (2014).
[52] I. Souza, N. Marzari, and D. Vanderbilt, Phys. Rev. B **65**, 035109 (2001).
[53] J. Coulter, R. Sundararaman, and P. Narang, Phys. Rev. B **98**, 115130 (2018).
[54] A. Habib, F. Florio, and R. Sundararaman, J. Opt. **20**, 064001 (2018).
[55] P. B. Allen, Phys. Rev. B **3**, 305 (1971).
[56] L. Novotny and B. Hecht, *Principles of Nano-Optics* (Cambridge University Press, Cambridge, England, 2012).
[57] T. Christensen, W. Yan, A.-P. Jauho, M. Soljačić, and N. A. Mortensen, Phys. Rev. Lett. **118**, 157402 (2017).